Synthesis and properties of heterografted toothbrushlike copolymers with alternating PEG and PCL grafts and tunable RAFT-generated segments

Journal:	*Polymer Chemistry*
Manuscript ID:	PY-ART-03-2014-000332.R1
Article Type:	Paper
Date Submitted by the Author:	31-Mar-2014
Complete List of Authors:	Tang, Dandan; Soochow University, Jiang, Xiao; Soochow University, Liu, Huanhuan; Soochow University, Li, Cangxia; Soochow University, Zhao, Youliang; Soochow University, College of Chemistry, Chemical Engineering and Materials Science

Cite this: DOI: 10.1039/c0xx00000x

www.rsc.org/xxxxxx

ARTICLE TYPE

Synthesis and properties of heterografted toothbrushlike copolymers with alternating PEG and PCL grafts and tunable RAFT-generated segments†

Dandan Tang, Xiao Jiang, Huanhuan Liu, Cangxia Li and Youliang Zhao*

Received (in XXX, XXX) Xth XXXXXXXXX 20XX, Accepted Xth XXXXXXXXX 20XX
DOI: 10.1039/b000000x

Synthesis and properties of novel (A-*g*-D)(B-*alt*-C)$_m$D-type heterografted toothbrushlike copolymers were described. The target copolymers comprised three types of building blocks involving terminal comblike block with quaternization bridging poly(*N,N*-dimethylaminoethyl methacrylate) (PDMA, A) substrate and D grafts, middle comblike block with poly(styrene-*alt*-maleimide) backbone and alternating PEG (B) and PCL (C) grafts, and terminal D segment involving poly(*N*-isopropylacrylamide) (PNIPAM), poly(methyl methacrylate) (PMMA), polystyrene (PSt), and poly(methyl acrylate) (PMA). The combination of quaternization and RAFT processes allowed for controlled synthesis of the target copolymers with precise microstructure and tunable composition and grafting density. With the change in macromolecular architecture, chemical composition and grafting density, toothbrushlike copolymers were liable to exhibit different physicochemical properties such as chain relaxation, melting, crystallization, and self-assembly behaviors. The introduction of chemical heterogeneity into non-responsive toothbrushlike copolymers could endow polymer films with notable thermo-dependent wettability due to accelerated surface penetration and reconstruction. Meanwhile, the drug release properties of PNIPAM-based aggregates were significantly affected by temperature, additives and end group, revealing the potential as promising controlled delivery vehicles. In addition to developing a general approach to construction of sequence-defined toothbrushlike copolymers with multicomponent grafts and variable grafting densities, our study further extended their potential applications in stimuli-sensitive surface and biomedical materials via changing the compatibility and supramolecular interactions.

Synthesis of precisely controlled polymer architectures has been an enduring topic in current polymer science.[1–12] The continued development of new routes for polymer synthesis has promoted the rapid development in some fields involving materials science, bioscience and nanotechnology. Tremendous progress in linkage chemistry and living/controlled polymerization techniques have provided access to a wide range of complex macromolecular architectures such as block, star, and graft copolymers with excellent control over molecular weight, chain architecture and functionality.[1–12] Considering the critical roles of structural complexity and special function in advanced polymer materials, it is of great importance to further explore facile approaches to construction of novel topological macromolecules.

As an important member in polymer family, graft polymer has attracted much attention due to its unique properties and potential applications such as templates for nanomaterials[13–15] and molecular tensile machines.[16–18] Depending on macromolecular parameters such as grafting density, chain length, length/width ratio, and chemical composition, graft polymers are liable to phase separate into a wide range of structures and morphologies, and thus they can exhibit variable physicochemical properties involving different chain morphologies, unusual mechanical properties, and lower viscosity and glass transition temperature as compared with their linear analogues.[7–12] It has revealed that the densely grafted molecular bottle brushes can exhibit wormlike single chain morphology, and loosely grafted polymers usually possess morphologies similar to star or other architectures.[19–22] Thus far, three general methods comprising "grafting onto", "grafting through" and "grafting from" routes have been developed for the synthesis,[7–12,19–29] and recent advances in controlled synthesis of stimuli-responsive graft polymers further extend the ranges of functionalities and applications.[30,31]

Considering that monomer sequence regulation usually plays a key role in biology and is a prerequisite for crucial features of life, sequence-controlled polymers have been developed to mimic the structural and functional complexity of biopolymers.[32–42] The current techniques have allowed synthetic polymers with controlled sequences, which may have many scientific and technological implications for eventual dreams towards bionic data storage, structural control, and self-replication.[33] Although most sequence-regulated synthetic polymers are of linear architecture, complex graft polymers and their derivatives with regular sequence of pendent chains have emerged. For instance, Chen and coworkers synthesized polymer brushes with

alternating grafts comprising linear chains and dendritic wedges,[43–46] Moughton et al. reported on one-step synthesis of $A(BC)_n$-type block polymer miktobrushes,[47] and we prepared mono or multi-cleavable A_mB_n comblike copolymers,[48] $A(BC)_mD$ comblike-linear block copolymers,[49] symmetric $A_{2m}B_{2n}C_2$ starlike terpolymers,[50] and $A_mB_nC_o$ dendritic toothbrushlike copolymers[51] with alternating PEG and PCL grafts, in which the radical copolymerization of styrenic and maleimidic comonomers were used to generate the alternating microstructures in all cases. To date, the examples of graft polymers with multicomponent grafts and different grafting densities are very scarce, and it is timely to further enrich the types of sequence-defined graft polymers and explore the direct correlation between structure and function. On one hand, the introduction of multiple compositions in pendent chains can not only endow polymers with tunable functions and responsive properties but favor the formation of complex nanoobjects involving multicompartment micelles via self-assembly in selective solvents.[52–57] The combination of two or more types of side chains with different properties can lead to new insights into the nature of macromolecules and polymer materials with exceptional properties,[58] and the results from molecular simulations reveal that they may exist as unimolecular cylinders of Janus-type or Janus dumbbell-type in the presence of phase-separated side chains.[59] On the other hand, the combination of loose and dense grafts in one macromolecule may bring more intriguing bulk, solution and interface properties due to the tunable stiffness and amphiphilicity originating from the differences in length/width and hydrophilic/hydrophobic ratios, grafting densities, and building block ratios.[7–31,43]

This study aims at facile synthesis and properties of (A-*g*-D)(B-*alt*-C)$_m$D-type heterografted toothbrushlike copolymers with multicomponent grafts and two kinds of grafting densities, in which four step reactions comprising quaternization and reversible addition-fragmentation chain transfer (RAFT)[60] process were used for the synthesis (Scheme 1). 2-Cyanopropan-2-yl dithiobenzoate (CPDB) mediated RAFT polymerization of *N,N*-dimethylaminoethyl methacrylate (DMA) afforded couplable PDMA (A), and followed by RAFT copolymerization of *α*-methoxy-*ω*-vinylbenzyl poly(ethylene glycol) (St-PEG) and maleimidic poly(*ε*-caprolactone) (MI-PCL) to generate A(B-*alt*-C)$_m$ toothbrushlike copolymer. After introducing variable CTA functionality via quaternization between DMA unit and 3-bromopropyl 4-(benzodithioyl)-4-cyanopentanoate (BBCP), the third RAFT process was performed to synthesize the target toothbrushlike copolymers with various D segments. The synthesized amphiphilic copolymers possessed rich compositions, variable chain lengths, and versatile building blocks comprising terminal quaternized comblike block with tunable grafting density, middle block with alternating PEG and PCL grafts, and terminal D segment as the handle. The resultant copolymers were characterized by ^{1}H NMR spectra, GPC-MALLS, and DSC. In addition, the surface wettability of copolymer films and drug loading and release properties of PNIPAM-based copolymer aggregates were investigated.

Some factors were considered to select the specific components. Biocompatible PEG and biodegradable PCL were selected due to their wide applications in biomaterials, PDMA bearing tertiary amine groups was chosen as a couplable agent to introduce tunable CTA functionality for attachment of other pendent chains, PNIPAM was used as a model stimuli-responsive segment to evaluate the potential of toothbrushlike copolymers in smart materials, and other polystyrene and poly(meth)acrylate segments were utilized to study the effects of chemical composition on physicochemical properties of the target heterografted polymers. The originality and novelty of this study primarily lie in three aspects. First, a new method comprising combined "grafting through" and "grafting from" techniques to form grafts and Menschutkin reaction to introduce variable CTA functionality was developed to synthesize novel (A-*g*-D)(B-*alt*-C)$_m$D-type toothbrushlike copolymers, which further enriches the family of sequence-regulated graft polymers and their derivatives. Second, the presence of three types of graft chains and different grafting densities involving alternating pendent chains allowed toothbrushlike copolymers with versatile compositions and tunable parameters and functions, evident from their unique physicochemical properties involving chain relaxation, melting, crystallization, and self-assembly behaviors and thermo-sensitive wettability of polymer films. Last, PNIPAM-based copolymer aggregates could efficiently act as nanocarriers to encapsulate hydrophobic drug, and the drug release kinetics was strongly dependent on some factors such as temperature, additives and end group, revealing the great potential of heterografted copolymer in smart drug delivery systems.

Experimental section

Materials

All solvents, monomers, and other chemicals were purchased from Sigma-Aldrich unless otherwise stated. *ε*-Caprolactone (CL, 99%) was distilled from calcium hydride under reduced pressure. Styrene (St, 99%), 4-vinylbenzyl chloride (VBC, 90%), *N,N*-dimethylaminoethyl methacrylate (DMA, 99%), methyl acrylate (MA, 99%) and methyl methacrylate (MMA, 99%) were passed through a basic alumina column to remove the inhibitor. *N*-Isopropylacrylamide (NIPAM, 97%) was recrystallized twice from mixtures of hexane and toluene. 2,2′-Azobis(isobutyronitrile) (AIBN) was recrystallized twice from ethanol. Monomethoxy poly(ethylene glycol) (MPEG, M_n = 750 g mol^{-1}, Fluka) was dried by azeotropic distillation in the presence of toluene, and 3-bromopropanol (99%) was distilled under reduced pressure. *N,N*′-Dicyclohexylcarbodiimide (DCC) and 4-dimethylaminopyridine (DMAP) were purchased from Sinopharm Chemical Reagent Co., Ltd. and used as received. Dichloromethane (DCM) and dioxane were dried and distilled over CaH_2. Tetrahydrofuran (THF) and toluene were distilled over sodium and benzophenone and stored under nitrogen. *α*-Methoxy-*ω*-vinylbenzyl poly(ethylene glycol) (St-PEG),[46] maleimidic poly(*ε*-caprolactone) (MI-PCL, $M_{n,NMR}$ = 1850 g mol^{-1}, PDI = 1.08),[51] 2-cyanopropan-2-yl dithiobenzoate (CPDB),[60] 3-bromopropyl 4-(benzodithioyl)-4-cyanopentanoate (BBCP),[61] 4-cyanopentanoic acid dithiobenzoate (4-CPDB),[62] and *N*-(2-hydroxyethyl)maleimide (HEMI)[63] were synthesized and purified according to literature procedures.

Synthesis of PDMA(PEG-*alt*-PCL)$_m$ copolymer

CPDB (0.111 g, 0.50 mmol), DMA (2.36 g, 15 mmol), and AIBN (16.4 mg, 0.10 mmol) were added to a Schlenk tube, and dioxane

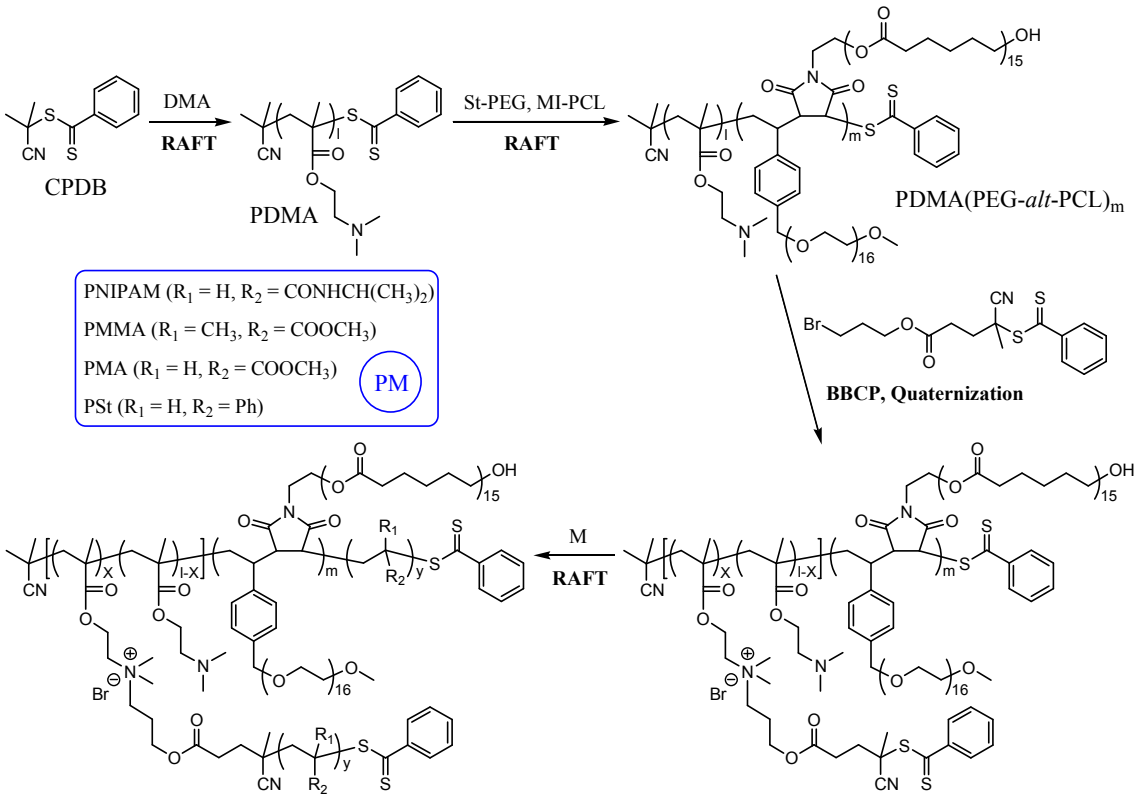

Scheme 1 Synthetic routes to (PDMA-*g*-PM)(PEG-*alt*-PCL)$_m$PM heterografted toothbrushlike copolymers by combination of RAFT process and Menschutkin reaction

was added until the total volume was 5.0 mL. The contents were degassed with bubbled nitrogen for 15 min, and then the polymerization was performed at 70 °C for 14 h. The mixture was concentrated and precipitated into cold hexane, and 2.20 g (88.6% conversion) of PDMA was obtained. $M_{n,GPC}$ = 3600 g mol^{-1}, PDI = 1.08, and $M_{n,NMR}$ = 4560 g mol^{-1}. ^{1}H NMR ($CDCl_3$): δ 7.86, 7.52, 7.36 (m, Ph*H*), 4.06 (s, CH_2O of PDMA), 2.56 (s, CH_2N of PDMA), 2.28 (s, (CH_3)$_2$N of PDMA), 0.6-2.2 (other CH_2 and CH_3 resulting from CTA and PDMA backbone). FT-IR (KBr): 3432, 2947, 2861, 2822, 2770, 1728, 1459, 1386, 1365, 1272, 1241, 1150, 1099, 1059, 1043, 1017, 963, 851, 780, 748, 692 cm^{-1}.

PDMA (0.91 g, 0.20 mmol), St-PEG (2.60 g, 3.0 mmol), MI-PCL (5.55 g, 3.0 mmol), and AIBN (6.6 mg, 0.04 mmol) were added to a Schlenk tube, and dry dioxane was added until the total volume was 20.0 mL. The contents were degassed with bubbled nitrogen for 30 min, and the polymerization was performed at 70 °C for 17 h. The mixture was concentrated and precipitated into cold hexane, and 8.13 g (88.6% conversion) of PDMA(PEG-*alt*-PCL)$_m$ (T1) was isolated. $M_{n,LS}$ = 37500 g mol^{-1}, PDI = 1.09, and $M_{n,NMR}$ = 36400 g mol^{-1}. ^{1}H NMR ($CDCl_3$): δ 6.5-8.0 (m, Ar*H* of St-PEG unit and terminal Ph*H*), 4.51 (s, ArCH_2O of St-PEG unit), 4.06 (m, CH_2O of PDMA and MI-PCL unit), 3.65 (m, CH_2CH_2O of St-PEG unit, and C*H* and CH_2N of MI-PCL unit), 3.38 (s, CH_3O of St-PEG unit), 2.57 (m, CH_2N of PDMA), 2.31 (m, (CH_3)$_2$N of PDMA, and CH_2CO of MI-PCL unit), 0.6-2.2 (m, other C*H*, CH_2 and CH_3 resulting from CTA and polymer backbone). FT-IR (KBr): 3454, 2941, 2868, 2775, 1732, 1642, 1460, 1394, 1353, 1239, 1156, 11008, 1041, 954, 849, 743 cm^{-1}.

Synthesis of BBCP modified PDMA(PEG-*alt*-PCL)$_m$ copolymers with tunable CTA functionality

Quaternization between T1 and BBCP was performed to generate toothbrushlike copolymers with enhanced CTA functionality (f_{CTA}). In a typical run, 1.82 g (1.38 mmol DMA unit) of T1 and 0.276 g (0.69 mmol) of BBCP were added to 9.1 mL of dry DMF under nitrogen. The mixture was heated at 60 °C for 20 h, concentrated and precipitated into hexane thrice. After vacuum drying, T2 (f_{CTA} = 6.0) was isolated in 96% yield, and degree of quaternization (DQ) was determined to be 18.1% by ^{1}H NMR analysis. Other copolymers T3 ([BBCP]$_0$:[DMA]$_0$ = 1.0, f_{CTA} = 10.8, DQ = 35.5%) and T4 ([BBCP]$_0$:[DMA]$_0$ = 2.0, f_{CTA} = 21.2, DQ = 73.2%) were synthesized according to similar procedures. ^{1}H NMR ($CDCl_3$): δ 7.92, 7.58, 7.41 (m, Ph*H*), 6.5-7.2 (m, Ar*H* of St-PEG unit), 4.50 (s, ArCH_2O of St-PEG unit), 4.27 (m, CH_2O), 4.06 (m, CH_2O of PDMA and MI-PCL unit), 3.0-3.9 (m, CH_2N$^+$(CH_3)$_2$CH_2, CH_2CH_2O and CH_3O of St-PEG unit, and C*H* and CH_2N of MI-PCL unit), 2.4-2.8 (m, CH_2N of PDMA, and CH_2CH_2COO beside dithiobenzoate), 2.31 (m, (CH_3)$_2$N of PDMA, and CH_2CO of MI-PCL unit), 0.6-2.2 (m, other C*H*, CH_2 and CH_3 resulting from CTA and polymer backbone). FT-IR (KBr): 3452, 2941, 2867, 1733, 1641, 1462, 1394, 1354, 1238, 1160, 1105, 1042, 989, 952, 850, 743, 690 cm^{-1}.

Synthesis of toothbrushlike copolymers with tunable number of PM segments by chain extension polymerization

In a typical polymerization, T2 (0.373 g, 0.10 mmol dithiobenzoate), NIPAM (0.904 g, 8.0 mmol), and AIBN (3.3 mg, 0.02 mmol) were added to a Schlenk tube, and dry DMF was added until the total volume was 8.0 mL. After degassing with bubbled nitrogen for 15 min, the contents were polymerized at 60 ^{o}C for 15 h. The mixture was concentrated and precipitated into cold diethyl ether thrice, and 0.676 g (33.5% conversion) of (PDMA-*g*-PNIPAM)(PEG-*alt*-PCL)$_m$PNIPAM (T6) was obtained after vacuum drying. $M_{n,LS}$ = 72500 g mol^{-1}, PDI = 1.10, and $M_{n,NMR}$ = 72000 g mol^{-1}. Other heterografted toothbrushlike copolymers were synthesized and purified according to similar procedures.

(PDMA-*g*-PNIPAM)(PEG-*alt*-PCL)$_m$PNIPAM (T5-T7): ^{1}H NMR ($CDCl_3$): δ 7.96, 7.56, 7.39 (m, Ph*H*), 6.0-7.2 (Ar*H* of St-PEG unit and N*H* of PNIPAM), 4.51 (m, ArCH_2O of St-PEG unit), 4.26 (CH_2O), 4.06 (m, CH_2O of PDMA and MI-PCL unit, and C*H* of PNIPAM), 3.1-3.9 (m, CH_2N$^+$(CH_3)$_2$CH_2, CH_2CH_2O and CH_3O of St-PEG unit, and C*H* and CH_2N of MI-PCL unit), 0.6-3.0 (m, other C*H*, CH_2 and CH_3 resulting from CTA, PDMA, MI-PCL unit, polymer backbone and PNIPAM). FT-IR (KBr): 3438, 3069, 2970, 2935, 2872, 1735, 1649, 1549, 1461, 1388, 1367, 1240, 1168, 1104, 1044, 952, 881, 843, 733, 701 cm^{-1}.

(PDMA-*g*-PMMA)(PEG-*alt*-PCL)$_m$PMMA (T8): ^{1}H NMR ($CDCl_3$): δ 7.89, 7.53, 7.37 (m, Ph*H*), 6.5-7.2 (Ar*H* of St-PEG unit), 4.51 (m, ArCH_2O of St-PEG unit), 4.26 (CH_2O), 4.06 (t, *J* 6.8, CH_2O of PDMA and MI-PCL unit), 3.0-3.9 (m, CH_2N$^+$(CH_3)$_2$CH_2, CH_2CH_2O and CH_3O of St-PEG unit, C*H* and CH_2N of MI-PCL unit, and CH_3O of PMMA), 2.57 (m, CH_2N of PDMA), 2.2-2.5 (m, (CH_3)$_2$N of PDMA, and CH_2CO of MI-PCL unit), 0.6-2.2 (m, other C*H*, CH_2 and CH_3 resulting from CTA, polymer backbone and PMMA). FT-IR (KBr): 3444, 2950, 2870, 1732, 1643, 1483, 1453, 1390, 1358, 1273, 1243, 1193, 1149, 1101, 1043, 987, 959, 913, 844, 808, 749, 690 cm^{-1}.

(PDMA-*g*-PSt)(PEG-*alt*-PCL)$_m$PSt (T9): ^{1}H NMR ($CDCl_3$): δ 7.85, 7.52, 7.46 (m, Ph*H*), 6.0-7.2 (Ar*H* of St-PEG unit and Ph*H* of PSt), 4.6-5.0 (broad, C*H*S), 4.51 (m, ArCH_2O of St-PEG unit), 4.26 (CH_2O), 4.06 (t, *J* 6.8, CH_2O of PDMA and MI-PCL unit), 3.0-3.9 (m, CH_2N$^+$(CH_3)$_2$CH_2, CH_2CH_2O and CH_3O of St-PEG unit, and C*H* and CH_2N of MI-PCL unit), 2.57 (m, CH_2N of PDMA), 2.2-2.5 (m, (CH_3)$_2$N of PDMA, and CH_2CO of MI-PCL unit), 0.6-2.2 (m, other C*H*, CH_2 and CH_3 resulting from CTA, polymer backbone and PSt). FT-IR (KBr): 3416, 3082, 3060, 3026, 2922, 2853, 1732, 1600, 1493, 1452, 1384, 1353, 1260, 1104, 1029, 949, 803, 758, 699 cm^{-1}.

(PDMA-*g*-PMA)(PEG-*alt*-PCL)$_m$PMA (T10): ^{1}H NMR ($CDCl_3$): δ 7.98, 7.55, 7.40 (m, Ph*H*), 6.5-7.2 (Ar*H* of St-PEG unit), 4.84 (t, *J* 7.6, C*H*S), 4.51 (m, ArCH_2O of St-PEG unit), 4.26 (CH_2O), 4.06 (t, *J* 6.8, CH_2O of PDMA and MI-PCL unit), 3.0-3.9 (m, CH_2N$^+$(CH_3)$_2$CH_2, CH_2CH_2O and CH_3O of St-PEG unit, C*H* and CH_2N of MI-PCL unit, and CH_3O of PMA), 0.6-2.8 (m, other C*H*, CH_2 and CH_3 resulting from CTA, PDMA, PMA, MI-PCL unit and polymer backbone). FT-IR (KBr): 3453, 2952, 2869, 1735, 1642, 1449, 1387, 1353, 1261, 1195, 1164, 1105, 1045, 958, 829, 764, 690 cm^{-1}.

Cleavage of PSt grafts from toothbrushlike copolymer

To the solution of T9 (0.30 g) in THF (10 mL) were added ethanol (3.6 mL), water (0.4 mL), and KOH (0.80 g) under nitrogen, and then the mixture was refluxed for 60 h. The solution was concentrated under reduced pressure and neutralized with dilute HCl. The mixture was partitioned between water and dichloromethane. After washing with deionized water thrice, the organic phase was collected and dried with $MgSO_4$. After concentration and precipitation into cold methanol, 0.12 g (82% yield) of PSt was obtained. $M_{n,th}$ = 4580 g mol^{-1}, $M_{n,GPC}$ = 4610 g mol^{-1}, PDI = 1.14.

Formation of self-assembled and DOX-loaded copolymer aggregates

The copolymer aggregates were prepared by a dialysis method. Briefly, T6 (5.0 mg) was dissolved in 1.0 mL of DMSO and stirred for 2 h at room temperature. Then, the polymer solution was added dropwise into 9.0 mL of phosphate buffered saline (PBS, pH 7.4, 50 mM) solution under vigorous stirring. Two hours later, the solution was transferred into dialysis membrane tubing (MWCO 100 kDa) and dialyzed against PBS solution for 24 h to remove the organic solvent. The hydrodynamic diameter (D), particle size distribution (PD), and morphology of aggregates were determined by DLS and TEM, respectively.

In a typical run to fabricate DOX-loaded aggregates, T6 (50.0 mg) and doxorubicin hydrochloride (DOX·HCl, 10.0 mg) were dissolved in 10.0 mL of DMSO, and followed by addition of about 3.0 mg of triethylamine. After stirring at room temperature for 2 h, the mixture was added dropwise to 90.0 mL of PBS solution (pH 7.4, 50 mM). The solution was stirred for an additional 6 h and dialyzed against PBS solution for 24 h (MWCO 10 kDa). The amount of DOX was determined using fluorescence (FLS920) measurements (excitation at 480 nm and emission at 560 nm). On the basis of fluorescence analysis, the drug loading capacity (DLC) of aggregates was calculated as the weight ratio of actual drug to drug-loaded aggregates, and the drug loading efficiency (DLE) of aggregates was calculated as the weight ratio of actual and added drug content.

In vitro drug release from DOX-loaded aggregates

In a typical run, four portions of DOX-loaded T6 aggregates in PBS solution (3.0 mL, pH 7.4) were put into a dialysis bag (MWCO 10 kDa), which were then immersed into 20 mL of (a) PBS solution (50 mM, pH 7.4) with 10 mM DTT or (b) normal PBS solution at 25 or 37 ^{o}C. The tubes were subjected to constant shaking at a fixed temperature. At desired time intervals, 3.0 mL of media outside the dialysis bag were taken for fluorescence measurement and 3.0 mL of fresh media were replenished. The amount of DOX released from aggregates was measured by fluorescence measurement (excitation at 480 nm) at room temperature. All release experiments were performed in triplicate, and the results presented are the average data with standard deviations. Other drug release experiments were conducted according to similar procedures.

Characterization

Apparent molecular weight ($M_{n,GPC}$) and polydispersity (PDI) of linear polymers were measured on a Waters 150-C gel permeation chromatography (GPC) using three Ultrastyragel

columns (pore size 50, 100, and 1000 nm, with molecular weight ranges of 100−10000, 500−30000, and 5000−600000 g mol^{-1}, respectively) with 10 μm bead size at 35 °C. THF was used as an eluent at a flow rate of 1.0 mL min^{-1}, and the samples were calibrated with PSt (for PSt) or PMMA (for other samples) standard samples. GPC with multiple angle laser scattering detection (GPC-MALLS) was used to determine the absolute number-average molecular weight ($M_{n,LS}$) of nonlinear polymers, in which GPC was conducted in DMF at 40 °C with a flow rate of 1.0 mL min^{-1}, and three MZ-Gel SDplus columns (pore size 10^3, 10^4 and 10^5 Å, with molecular weight ranges of 1000−40000, 4000−500000, and 10000−2000000, respectively) with 10 μm bead size were used. Detection systems consisted of a RI detector (Optilab rEX) and a multiangle (14°−145°) laser light scattering detector (DAWN HELLOS) with the He−Ne light wavelength at 658.0 nm. The refractive index increment d*n*/d*c* for samples were measured off-line by Optilab rEX refractive index detector (λ = 658 nm) at 25 °C using a series of different concentration solutions. Data were collected and processed by use of ASTRA software from Wyatt Technology, and molecular weights were determined by the triple detection method. ^{1}H (400 MHz) spectra were recorded on a Varian spectrometer at 25 °C using $CDCl_3$ as a solvent. Fourier Transform Infrared (FT-IR) spectra were recorded on a Perkin-Elmer 2000 spectrometer using KBr discs. Dynamic light scattering (DLS) measurements were carried out at 25 °C using Zetasizer Nano-ZS from Malvern Instruments equipped with a 633 nm He–Ne laser using back-scattering detection, and the micellar solutions were filtered through a 450 nm syringe filter before measurements. The water-repellent and adhesive properties of water droplets on the sample surfaces were characterized using an optical contact-angle meter system (Kino SL200C). UV-vis absorption spectra were recorded on a Shimadzu UV-3150 spectrophotometer using a heating rate of 1 °C min^{-1}, in which the transmittance at 500 nm was used to determine the cloud points, and the temperature of the cell was regulated to ±0.1 °C by a circulating water bath. Differential scanning calorimetry (DSC) analysis was performed under a nitrogen atmosphere on Q200 DSC (TA Instruments - Waters LLC) with a heating rate of 10 °C min^{-1}. Fluorescence spectroscopy was recorded at 25 °C on a FLS920 fluorescence spectrometer. Transmission electron microscopy (TEM) images were obtained through a Hitachi H-600 electron microscope.

Results and discussion

Synthesis of (A-*g*-D)(B-*alt*-C)$_m$D copolymers

First, couplable PDMA was obtained by CPDB mediated RAFT polymerization (run 2 of Table 1). In ^{1}H NMR spectrum (Fig. S1), characteristic signals were observed at 7.86, 7.52, 7.36 (Ph*H*), 4.06 (CH_2O of PDMA), 2.56 (CH_2N of PDMA), and 2.28 ppm ((CH_3)$_2$N of PDMA and terminal CH_2CO). The GPC trace of PDMA exhibited symmetric distribution (PDI = 1.08, Fig. S2), and the $M_{n,NMR}$ value ($M_{n,NMR}$ = 4560 g mol^{-1}, DP$_{DMA}$ = 27.6) determined by comparing the integrated areas at 7.86 and 4.06 ppm was in good accordance with the theoretical value.

Second, PDMA acted as a macro CTA to mediate RAFT copolymerization of St-PEG ($M_{n,NMR}$ = 870 g mol^{-1}, PDI = 1.04) and MI-PCL ($M_{n,NMR}$ = 1850 g mol^{-1}, PDI = 1.08, Fig. S2 and Fig. S3), and PDMA(PEG-*alt*-PCL)$_m$ copolymer (T1) was obtained. In ^{1}H NMR spectrum (Fig. 1), typical signals were observed at 4.51 (ArCH_2O of St-PEG unit), 4.06 (CH_2O of PDMA and MI-PCL unit), 3.65 (CH_2CH_2O of St-PEG unit, and C*H* and CH_2N of MI-PCL unit), 3.38 (CH_3O of St-PEG unit), 2.57 (CH_2N of PDMA), and 2.31 ppm ((CH_3)$_2$N of PDMA, and CH_2CO of MI-PCL unit). The numbers of PEG and PCL grafts per copolymer were determined to be m_{PEG} = 12.0 and m_{PCL} = 11.6 by ^{1}H NMR analysis, which were in accordance with the expected alternating microstructure of poly(St-*alt*-MI) backbone. The M_n values of T1 determined by ^{1}H NMR ($M_{n,NMR}$ = 36400 g mol^{-1}) and GPC-MALLS ($M_{n,LS}$ = 37500 g mol^{-1}) were close, and both were similar to the expected value by assuming that the copolymer was of alternating styrenic and maleimidic sequences ($M_{n,th}$ = 37200 g mol^{-1}). T1 exhibited symmetric distribution in GPC trace (Fig. 2), with relatively low polydispersity (PDI = 1.09).

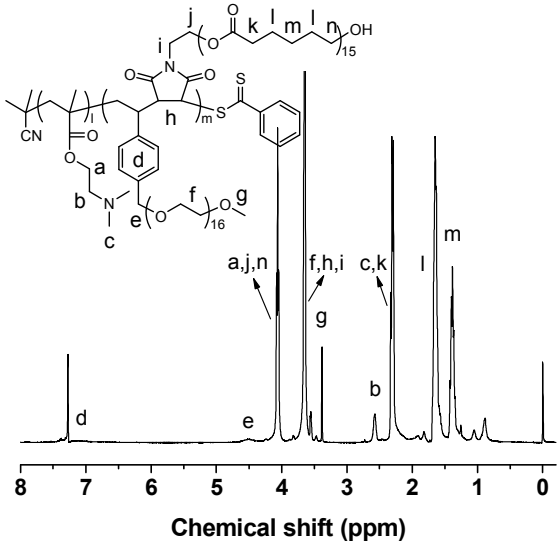

Fig. 1 ^{1}H NMR spectrum of PDMA(PEG-*alt*-PCL)$_m$ (T1, $l \approx 28$, $m \approx 12$) toothbrushlike copolymer.

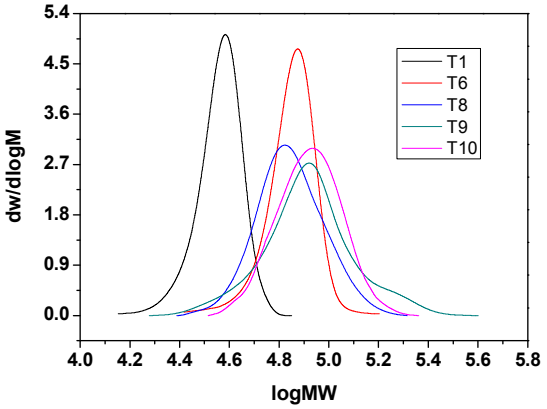

Fig. 2 GPC traces (normalized weight distribution) of T1 and (A-*g*-D)(B-*alt*-C)$_m$D (A = PDMA, B = PEG, C = PCL, D = PNIPAM (T6), PMMA (T8), PSt (T9) and PMA (T10)) copolymers.

Table 1 Results for synthesis of MI-PCL macromonomer (run 1), PDMA macro CTA (run 2) and A(B-*alt*-C)$_m$ (A = PDMA, B = PEG, C = PCL) toothbrushlike copolymer (T1, run 3) using various types of initiator (I) or chain transfer agent (CTA)[a]

run	polymer	I/CTA	M	C%[b]	$M_{n,th}$[c]	M_n[d]	PDI[d]	$M_{n,NMR}$ (DP)[e]
1	MI-PCL	HEMI	CL	98.1	1820	2800	1.08	1850 (15.0)
2	PDMA	CPDB	DMA	88.6	4400	3700	1.08	4560 (27.6)
3	T1	PDMA	St-PEG/MI-PCL	80.2	37200	37500	1.09	36400 (12.0/11.6)[f]

[a] Polymerization conditions: $[CL]_0:[HEMI]_0:[Sn(Oct)_2]_0$ = 15:1:0.1, $[CL]_0$ = 3.0 moL L^{-1}, in toluene at 90 °C for 20 h (run 1); $[DMA]_0:[CPDB]_0:[AIBN]_0$ = 30:1:0.2, $[DMA]_0$ = 3.0 moL L^{-1}, in dioxane at 70 °C for 14 h (run 2); $[St\text{-}PEG]_0:[MI\text{-}PCL]_0:[PDMA]_0:[AIBN]_0$ = 15:15:1:0.2, $[St\text{-}PEG]_0$ = 0.15 moL L^{-1}, in dioxane at 70 °C for 17 h (run 3). [b] Monomer conversion determined by gravimetry or ^{1}H NMR analysis. [c] Theoretical molecular weight. [d] Molecular weight and polydispersity estimated by GPC ($M_{n,GPC}$, runs 1 and 2) or determined by GPC-MALLS ($M_{n,LS}$, run 3). [e] Molecular weight ($M_{n,NMR}$) and degree of polymerization (DP) determined by ^{1}H NMR analysis. [f] Numbers of PEG and PCL grafts per copolymer (m_{PEG} = 12.0 and m_{PCL} = 11.6) as determined by ^{1}H NMR analysis.

Table 2 Results for synthesis of (A-*g*-D)(B-*alt*-C)$_m$D toothbrushlike copolymers via RAFT polymerization mediated by BBCP modified A(B-*alt*-C)$_m$ copolymers (T2-T4)[a]

sample	CTA	f_{CTA}	M	DP_0	t (h)	C%[b]	$M_{n,th}$[c]	$M_{n,LS}$[d]	PDI[d]	$M_{n,NMR}$ (DP)[e]
T5	T2	6.0	NIPAM	100	18	51.2	73100	74000	1.08	72300 (50.0)
T6	T3	10.8	NIPAM	80	15	33.5	73000	72500	1.10	72000 (25.9)
T7	T4	21.2	NIPAM	100	18	42.1	145300	148000	1.34	143900 (41.5)
T8	T3	10.8	MMA	80	15	34.3	70000	69200	1.12	68900 (26.5)
T9	T3	10.8	St	200	20	21.6	88800	93300	1.23	88200 (42.6)
T10	T3	10.8	MA	100	18	43.2	80400	84800	1.12	81600 (44.4)

[a] Polymerization conditions: $[M]_0:[dithiobenzoate]_0:[AIBN]_0 = DP_0$:1:0.2, $[M]_0$ = 1.0 mol L^{-1}, in DMF at 60 °C. [b] Monomer conversion determined by gravimetry or ^{1}H NMR analysis. [c] Theoretical molecular weight. [d] Molecular weight ($M_{n,LS}$) and polydispersity (PDI) determined by GPC-MALLS. [e] Molecular weight of toothbrushlike copolymer ($M_{n,NMR}$) and degree of polymerization (DP) of PM segments determined by ^{1}H NMR analysis.

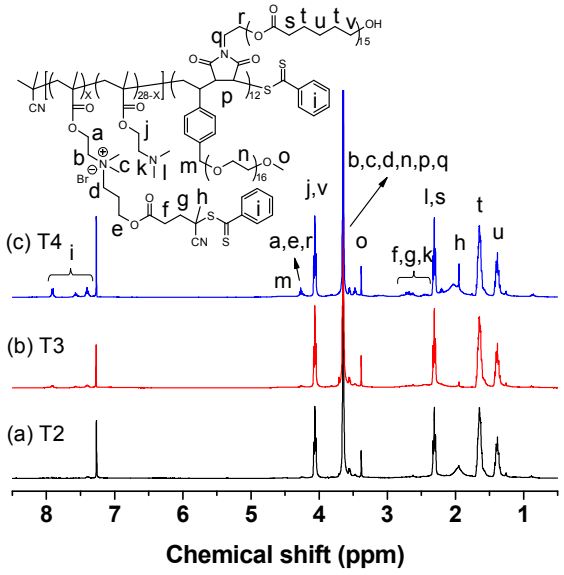

Fig. 3 ^{1}H NMR spectra of BBCP modified PDMA(PEG-*alt*-PCL)$_m$ copolymers (f_{CTA} = 6.0 (T2), 10.8 (T3) and 21.2 (T4)).

Third, BBCP was grafted onto PDMA segment of T1 via quaternization to form toothbrushlike copolymers T2-T4 with different CTA functionality (f_{CTA}). The quaternization was performed in DMF at 60 °C using feed ratio of BBCP to DMA unit ranging from 0.5 to 2, and the resultant macro CTA was obtained in high yield after precipitation and vacuum drying. After quaternization, the signals of PDMA segment at 4.06 (CH_2O of PDMA) and 2.56 ppm (CH_2N of PDMA) were weakened, and new signals resulting from the quaternized CTA appeared at 7.92, 7.58, 7.41 (m, Ph*H*), 4.27 (CH_2O), and 3.0-3.9 ppm ($CH_2N^+(CH_3)_2CH_2$) (Fig. 3). By comparing the integrated areas at 7.92 (Ph*H*) and 3.38 ppm (CH_3O of PEG segment), the f_{CTA} values were obtained to be 6.0 (T2), 10.8 (T3) and 21.2 (T4), corresponding to degree of quaternization (DQ = (f_{CTA} – 1)/DP_{DMA}) within 18.1%-73.2%. Toothbrushlike copolymers with DQ ranging from 0 to 1 could be achieved by changing reaction conditions owing to the high quaternization efficiency.

Last, (A-*g*-D)(B-*alt*-C)$_m$D copolymers (D = PNIPAM (T5-T7), PMMA (T8), PSt (T9) and PMA (T10)) were synthesized by RAFT polymerization mediated by T2 (for T5), T4 (for T7) and T3 (for other copolymers). In ^{1}H NMR spectra (Fig. 4), the signals at 2.4-2.8 ($COCH_2CH_2C(CH_3)(CN)S$, f and g of Fig. 3) and 1.94 ppm (terminal $CH_3C(CN)SC(=S)Ph$, Fig. 3h) completely disappeared, and characteristic signals appeared at

6.2-7.2 (Ph*H* of PSt), 4.06 (CH_2O of PDMA and PCL), 4.01 (*CH*NH of PNIPAM), 3.65 (CH_3O of PMA and CH_2CH_2O of PEG), 3.60 (CH_3O of PMMA), 2.57 (CH_2N of PDMA), 2.31 ($(CH_3)_2N$ of PDMA and CH_2CO of PCL), and 1.14 ppm (CH_3 of PNIPAM). The resultant copolymers had polydispersity indices in the range of 1.08-1.34 (Table 2), and their $M_{n,th}$, $M_{n,LS}$ and $M_{n,NMR}$ values were roughly comparable. These results revealed the chain extension polymerization was efficiently performed to generate the target copolymers, in which the graft number of D segments was dependent on the CTA functionality of their precursors.

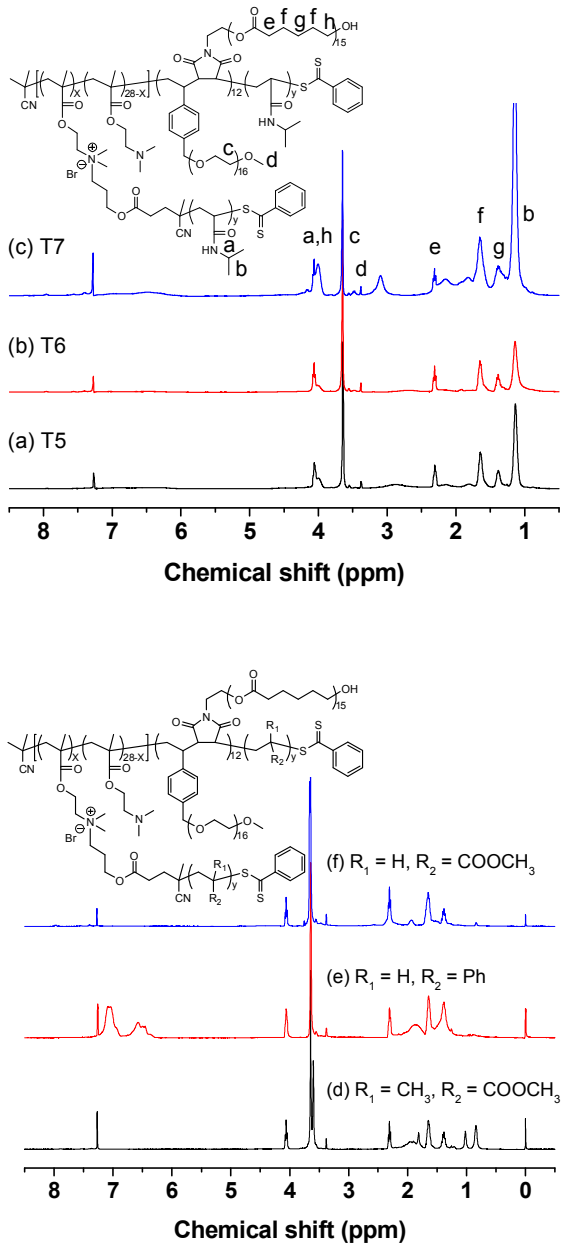

Fig. 4 ^{1}H NMR spectra of (PDMA-*g*-PM)(PEG-*alt*-PCL)$_m$PM copolymers: (a-c) T5-T7 (PM = PNIPAM); (d) T8 (PM = PMMA); (e) T9 (PM = PSt); (f) T10 (PM = PMA).

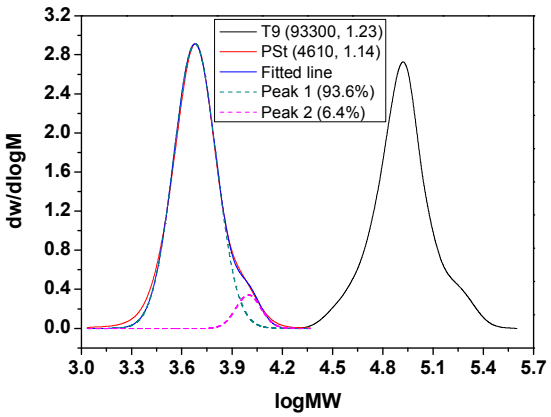

Fig. 5 GPC traces of T9 copolymer and grafted PSt segment obtained by hydrolysis.

Although toothbrushlike copolymers involving PNIPAM and PMA segments usually exhibited symmetric distribution in GPC traces, notable tailing and shoulder were observed in GPC traces of T8 and T9, suggesting the presence of side reactions such as radical coupling and disproportionation resulting from relatively high reactivity of chain radicals. To further reveal the uniformity of D segments, T9 was subjected to hydrolysis, and PSt was isolated by extraction and precipitation. GPC measurement revealed M_n and PDI of recovered PSt were 4610 g mol^{-1} and 1.14, and the M_n value was in good agreement with the expected one ($M_{n,th}$ = 4580 g mol^{-1}) by assuming all the dithiobenzoate functionalities had quantitatively participate in the RAFT process. The fitted lines as plotted in Fig. 5 revealed that about 6.4% of polystyryl radicals were subjected to coupling reaction to form dead chains during RAFT polymerization to grow PSt segments.

These results indicated the target (A-*g*-D)(B-*alt*-C)$_m$D copolymers with precise microstructures and controlled compositions could be achieved via four step reactions under optimized conditions. Owing to relatively limited number of ionic bonds locating between PDMA substrate and D grafts, the quaternized toothbrushlike copolymers did not exhibit abnormal solubility (Table S1). This general method comprising quaternization and RAFT processes has some advantages involving straightforward synthesis, versatile chemical compositions, tunable grafting density and chain length of D segments, and facile introduction of alternating B and C grafts.

DSC analysis

Glass transition (T_g) and melting (T_m) temperatures of typical toothbrushlike copolymers and their precursors were determined by DSC analysis (Fig. 6). In DSC curves, PDMA had one glass transition temperature (T_g) at 17.9 °C, St-PEG had one melting peak (T_m) at 29.5 °C,[51] MI-PCL exhibited one glass transition at -59.5 °C and two melting peaks at 39.9 and 47.9 °C, and the degree of crystallinity (X_c) was 49.8% (for St-PEG) and 60.2% (for MI-PCL). For T1 copolymer with different weight contents of PEG and PCL segments ($f_{w,PEG}$ = 0.247, $f_{w,PCL}$ = 0.545), one glass transition ($T_{g,PCL}$ = -59.6 °C) and two melting peaks ($T_{m,PEG}$ = 24.0 °C, $T_{m,PCL}$ = 41.1 °C) were observed, and the X_c values ($X_{c,PEG}$ = 37.7%, $X_{c,PCL}$ = 22.2%) were smaller than those of

corresponding macromonomers. The result was roughly comparable to that observed in densely grafted copolymer with polymethacrylate backbone and random PEG and PCL-*b*-PEG grafts,[64] in which the crystallizability of inner PCL blocks ($X_{c,PCL}$ = 24.3%, $f_{w,PCL}$ = 0.647) was significantly hindered by the presence of outlayer PEG segments. The reduced crystallizability in toothbrushlike copolymer could be ascribed to the increased crystalline imperfection of short pendent chains ($DP_{PEG} \approx 16$, $DP_{PCL} \approx 15$), in which the alternating sequences of PEG and PCL grafts in T1 copolymer could further hinder polymer chains from folding and rearrangement, resulting in enhanced structural confinement of polymer segments during crystallization than other random graft copolymers.

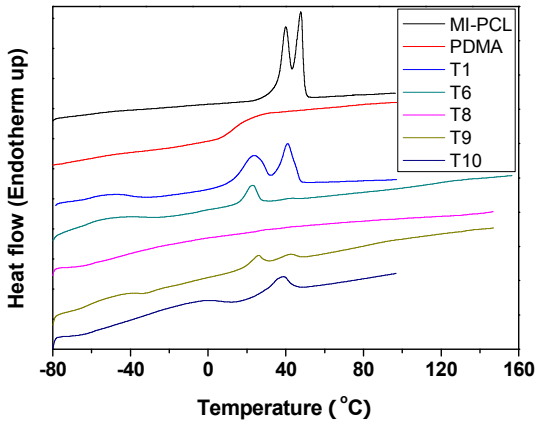

Fig. 6 DSC curves of typical toothbrushlike copolymers and their precursors.

As compared with A(B-*alt*-C)$_m$ copolymer, (A-*g*-D)(B-*alt*-C)$_m$D-type copolymer stands for another type of heterografted copolymer with RAFT-generated D segments as side chains of the first brush and the handle of the total toothbrush. Owing to increased compositions and more complex topologies, these copolymers are expected to exhibit more complex chain relaxation, melting and crystallization properties compared with their precursors. For quaternized toothbrushlike copolymers comprising PNIPAM (T6), PMMA (T8) and PMA (T10) segments, $T_{g,PCL}$ was noted in the range of -49.8 and -57.5 °C, and the other T_g appeared at 109.4 ($T_{g,PNIPAM}$), 66.6 ($T_{g,PMMA}$), and -5.8 °C ($T_{g,PMA}$), revealing the polar grafted segments were partly compatible in these copolymers. Although melting peaks appeared at 22.1 ($T_{m,PEG}$ of T6), 42.5 ($T_{m,PCL}$ of T6) and 38.5 °C ($T_{m,PCL}$ of T10), no significant melting peaks associated with PEG (for T8 and T10) and PCL (for T8) segments were noted in DSC curves. Because of the incompatibility among low-polarity PSt segments and other polar segments, T9 was liable to exhibit reduced glass transitions ($T_{g,PCL}$ = -63.6 °C, $T_{g,PSt}$ = 85.2 °C) and slightly enhanced melting peaks ($T_{m,PEG}$ = 25.8, $T_{m,PCL}$ = 42.0 °C) than T1. As compared with T1 ($X_{c,PEG}$ = 37.7%, $X_{c,PCL}$ = 22.2%), the degree of crystallinity of PEG and PCL grafts in quaternized copolymers ($X_{c,PEG}$ = 0-18.9%, $X_{c,PCL}$ = 0-9.71%, Table S2) was notably reduced. Although $f_{w,PEG}$ and $f_{w,PCL}$ values in each sample were very close, the $X_{c,PEG}$ and $X_{c,PCL}$ values were strongly dependent on the types of D segments. Our preliminary results indicated the introduction of PMMA and PMA segments could significantly hinder PEG grafts from crystallization, and the presence of PNIPAM and PMMA chains could remarkably restrict PCL crystallization. These results revealed that noncrystalline backbones, segments and end groups could act as "impurities" to affect the crystallization properties due to restricted folding and rearrangement of PEG and PCL segments. Moreover, the chemical compositions of D segments also played critical roles in crystallization due to the mutual interactions among crystalline and noncrystalline segments.

Therefore, the chain relaxation, melting and crystallization behaviors of heterografted toothbrushlike copolymers were significantly affected by alternating sequences, chemical compositions of pendent chains and macromolecular architecture.

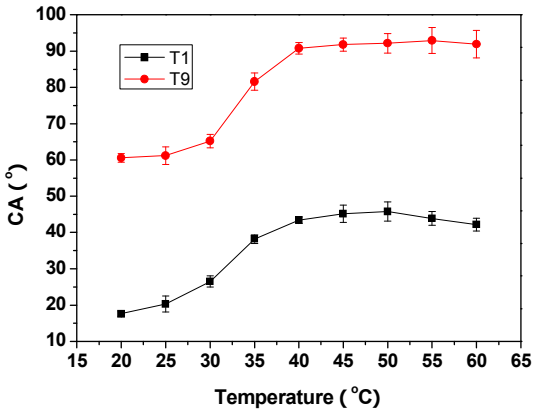

Fig. 7 Dependence of water contact angle of copolymer films on temperature.

Wettability properties of copolymer films

Chemical composition and macromolecular architecture can offer the possibility to tune the surface wettability of polymer films. To investigate the influence of temperature on wettability properties, various toothbrushlike copolymers were casted onto glass substrate to form copolymer films, and their water contact angles (CAs) were measured at different temperatures (Table 3). As temperature increased from 25 to 40 °C, the CA values of T1 film varied from 20.3° to 43.4°. The distinct CA (ΔCA = 23.1°) could be ascribed to increasing hydrophobicity of PDMA segment at elevated temperature (Fig. 7). For T5-T7 films bearing PNIPAM segments, the CA values at 25 °C were within 27.4-34.8°, and the CA difference (ΔCA = 18.8-20.1°) at 25 and 40 °C was roughly comparable to that of PNIPAM film (ΔCA = 19.1°), revealing the presence of thermo-dependent wettability. Although T8 and T10 films comprising PMMA and PMA segments did not exhibit notable CA gap at 25 and 40 °C (ΔCA = 5.0-7.8°), T9 film bearing PSt segments was of outstanding thermo-responsive surface properties (ΔCA = 29.6°) possibly originating from chemical heterogeneity and enhanced chain mobility within and beyond the melting range of PEG and PCL segments. As evidenced from the aforementioned DSC analysis, PMMA and PMA could be partly compatible with other polar segments, however, PSt was almost incompatible with PEG and PCL grafts due to its low polarity. With increasing temperature, PEG and

Table 3 Influence of temperature on water contact angles (CAs) of various polymer films

sample	type	CA (°, 25 °C)	CA (°, 40 °C)	ΔCA (°)
T1	A(B-*alt*-C)$_m$	20.3 ± 2.2	43.4 ± 0.9	23.1
T5	(A-*g*-D)(B-*alt*-C)$_m$D (D = PNIPAM)	27.4 ± 1.5	47.5 ± 2.1	20.1
T6	(A-*g*-D)(B-*alt*-C)$_m$D (D = PNIPAM)	33.7 ± 1.0	52.5 ± 2.3	18.8
T7	(A-*g*-D)(B-*alt*-C)$_m$D (D = PNIPAM)	34.8 ± 2.1	53.6 ± 1.8	18.8
T8	(A-*g*-D)(B-*alt*-C)$_m$D (D = PMMA)	68.5 ± 2.0	73.5 ± 2.5	5.0
T9	(A-*g*-D)(B-*alt*-C)$_m$D (D = PSt)	61.2 ± 2.4	90.8 ± 1.6	29.6
T10	(A-*g*-D)(B-*alt*-C)$_m$D (D = PMA)	45.8 ± 2.1	53.6 ± 2.2	7.8
PNIPAM	homopolymer	35.1 ± 1.9	54.2 ± 1.6	19.1
PMMA	homopolymer	74.5 ± 2.1	77.2 ± 1.8	2.7
PSt	homopolymer	90.2 ± 2.6	93.3 ± 2.2	3.1
PMA	homopolymer	65.5 ± 1.5	66.8 ± 2.1	1.3

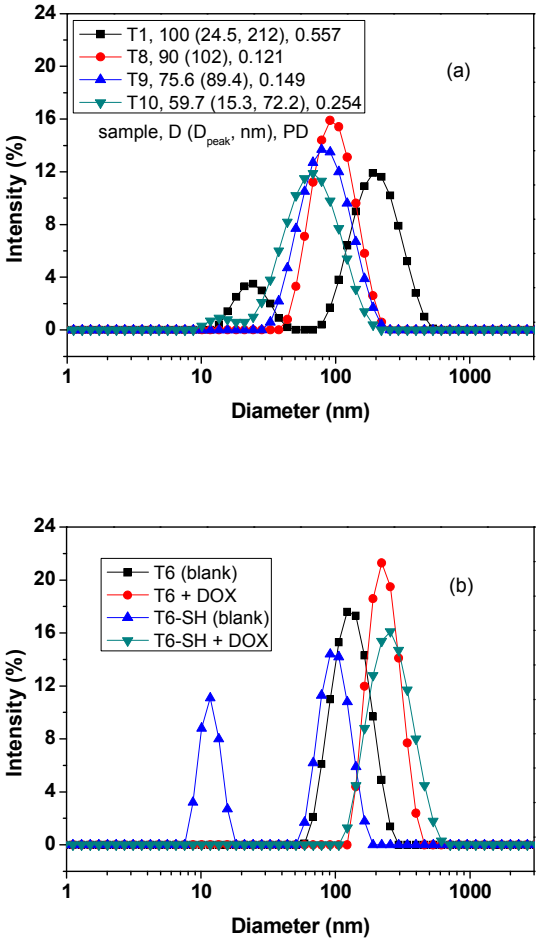

Fig. 8 DLS plots of blank and DOX-loaded aggregates (c = 0.50 mg mL^{-1}) formed from various copolymers in PBS solution (pH 7.4, 50 mM) at 37 °C.

PCL segments gradually melted, and PSt segments were liable to promptly remove into the outermost layer owing to poor compatibility and faster chain mobility, resulting in accelerated surface penetration and reconstruction. Consequently, copolymer film with PSt segments could exhibit more sensitive CA-T relationship than PMMA and PMA-based films. With increasing temperature, the CA value of T9 film was gradually increased from 61.2 ° (T = 25 °C) to 90.8° (T = 40 °C), and then it was almost constant until 60 °C or more (Fig. 7). These results indicated T9 film at 40-60 °C was liable to exhibit wettability property close to pure PSt film. Meanwhile, no significant change in transmittance of polymer solution (c = 1.0 mg mL^{-1}) was noted during 20 and 60 °C (Fig. S5), corresponding to lack of thermo-responsiveness of T9 aggregates in aqueous solution. Our results revealed that the introduction of chemical heterogeneity into non-responsive copolymers was liable to result in thermo-dependent surface properties, in which the surface wettability of polymer films could be efficiently adjusted by control over chemical composition and topological structure.

Formation of copolymer aggregates and influence of DTT and *α*-CD

To reveal the influence of chemical composition and topology on aggregation behaviors, self-assembly of various heterografted toothbrushlike copolymers was performed. Besides, multithiol-functionalized T6-SH was generated by aminolysis of T6 using hydrazine hydrate and acted as a typical sample to reveal the influence of various factors on aggregation behaviors and drug release properties.

After formation of copolymer aggregates at 37 °C by dialysis, DLS was used to determine their average hydrodynamic diameter (D), peak size (D$_{peak}$) and particle size distribution (PD). In DLS plots (Fig. 8a), T1 and T10 aggregates exhibited bimodal distribution with peak sizes at 24.5 and 212 nm (for T1), and 15.3 and 72.2 nm (for T10), the sizes of copolymer micelles given by DLS and TEM were similar, and TEM images indicated the aggregates were mixtures of unimolecular, normal or large compound micelles (a and d of Fig. S7). For T8 and T9 aggregates, monomodal distribution appeared in DLS plots, and

their particle parameters (D, D_{peak}, PD) were 90 nm, 102 nm, 0.121 (for T8), and 75.6 nm, 89.4 nm and 0.149 (for T9). TEM images revealed that T8 and T9 aggregates were multicompartment vesicles (b and c of Fig. S7), and the sizes (about 62 nm for T8 aggregates, and 45 nm for T9 aggregates) given by TEM images were smaller than those determined by DLS analysis due to significant shrinkage of polymer vesicles during drying.

T6 aggregates exhibited monomodal distribution in DLS plots, and their particle parameters (D, D_{peak}, and PD) were obtained as 125 nm, 135 nm, 0.195 at 37 °C (Fig. 8b), and 144 nm, 145 nm, 0.128 at 25 °C (Fig. 9a). TEM images in Fig. S8 revealed that T6 aggregates were normal and large compound micelles. The sizes of T6 aggregates at 25 °C given by DLS and TEM were similar; while the diameter of copolymer aggregates at 37 °C estimated by TEM (D ≈ 60 nm, Fig. S8b) was much lower than that given by DLS. The latter could be partly ascribed to the significant shrinkage of nanostructures in the dry state, in which the enhanced hydrophobic contents of T6 increased at higher temperature possibly resulted in aggregates with looser packing of polymer segments. At 37 °C, T6-SH aggregates showed bimodal distribution with peak sizes at 11.8 and 101 nm in DLS plots, and their D and PD values were 67.0 nm and 0.270, respectively (Table 4). These results revealed the self-assembly behaviors could be strongly affected by some factors involving chemical composition, topological structure, end group and temperature owing to their contribution to hydrophilic/ hydrophobic ratio, chain stacking, strength and types of mutual interactions.

The additives may significantly affect the stability of copolymer aggregates and even generate coassemblies owing to their roles in changing the microenvironment via intra- and inter-molecular interactions.[65–71] In this study, DTT and α-CD were chosen as typical additives to interact with T6 and T6-SH due to their potential in altering the strength of hydrogen-bonding interactions and van der Waals forces and formation of host-guest interactions among α-CD, PEG and PCL segments.[68–71] To reveal these phenomena, the additives (10 mM DTT and 1.0 mM α-CD) were added to the aqueous solution of T6 aggregates at 25 or 37 °C, and the DLS plots were continuously monitored. Lack of additives, T6 aggregates could be stably stored at the fixed temperature, and no significant change in DLS plots appeared after storage for 48 h (Fig. S9). In the presence of external additives, the average hydrodynamic sizes of aggregates notably increased to more than 200 nm, and D and PD of various aggregates were strongly dependent on time and temperature. As plotted in Fig. 9 and Fig. 10, the particle parameters varied gradually with extended time, and sometimes the DLS plots even exhibited bimodal distribution. Another finding was that the main peak sizes of aggregates in the presence of additives were remarkably higher than those of original aggregates although the D_{peak} and distribution values did not usually show a continuous increasing or decreasing tendency with prolonging time (Table S3). The hydrodynamic sizes of aggregates with DTT first increased from 215 (2 h) to 256 nm (10 h) and then dropped to 178 nm at 24 h, while the D values of aggregates using α-CD was liable to decrease from 311 nm at 2 h to 239 nm at 24 h. At 37 °C, the hydrodynamic sizes of aggregates with DTT varied between 204 and 296 nm, and the D values of aggregates using α-CD tended to increased from 362 nm at 2 h to 501 nm at 24 h. These results revealed that the addition of external additives could promote the reaggregation of copolymer aggregates due to the interactions among the additive and various polymer segments, which was more or less similar to the coassembly process. In the presence of DTT and α-CD, the remarkably changed D and PD values evidenced by DLS measurement indicated the reaggregation was dynamically performed. This phenomenon could be partly ascribed to the dynamic diffusion and coaggregation between additives and copolymer aggregates, in which the densely packed polymer segments in various aggregates were liable to hinder the hydrophilic additives from approaching the aggregates to form larger (co)aggregates via mutual interactions, while the reaggregation was gradually conducted during the diffusion process, and thus it usually took a long period of time to reach the thermodynamic equilibrium.

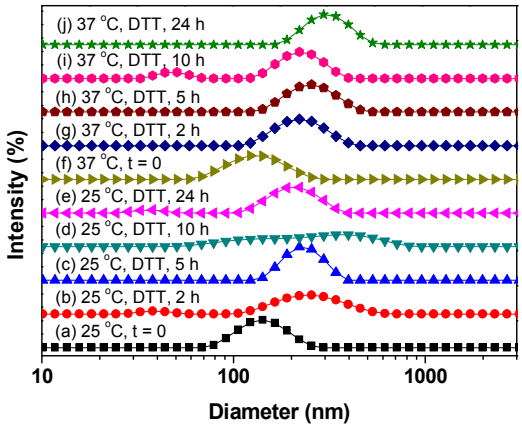

Fig. 9 DLS plots of T6 aggregates (c = 0.50 mg mL^{-1}) in PBS solution (50 mM, pH 7.4) with or without addition of 10 mM DTT at 25 or 37 °C.

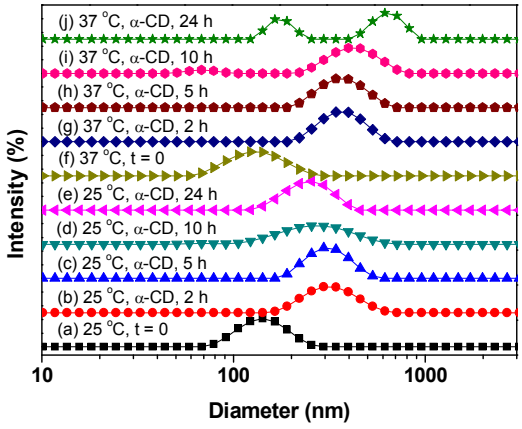

Fig. 10 DLS plots of T6 aggregates (c = 0.50 mg mL^{-1}) in PBS solution (50 mM, pH 7.4) with or without addition of 1.0 mM α-CD at 25 or 37 °C.

Table 4 Influence of end group on properties of copolymer aggregates at 37 °C

sample	D (nm)[a]	PD[a]	D_{peak} (nm)[a]	D (nm)[b]	PD[b]	D_{peak} (nm)[b]	DLC (%)	DLE (%)
T6	125	0.195	135	220	0.092	235	5.64	28.2
T6-SH	67.0	0.270	11.8, 101[c]	241	0.124	269	6.15	30.8

[a] Hydrodynamic diameter (D), particle size distribution (PD), and peak size (D_{peak}) of blank copolymer aggregates obtained by DLS analyses. [b] D, PD and D_{peak} values of DOX-loaded copolymer aggregates. [c] Bimodal distribution was observed.

Stimuli-triggered in vitro drug release from DOX-loaded copolymer aggregates

As well documented, some factors such as additives,[68–71] end group,[51,72–74] and macromolecular architecture[64,75–80] can play important roles in drug delivery systems. To reveal the potential of heterografted copolymers in bioscience, T6 and T6-SH aggregates were chosen for loading and release of DOX, and the effects of temperature, additives (DTT and *α*-CD) and end group on drug release properties were investigated.

A model anticancer drug DOX was encapsulated into copolymer aggregates at 37 °C by dialysis method. After loading the drug at 37 °C, copolymer aggregates were of hydrodynamic sizes remarkably increased to 220 (for T6) and 241 nm (for T6-SH), and unimodal distribution with reduced PD values was noted in DLS plots (Table 4 and Fig. 8). As determined by fluorescence analysis, the drug loading capacity (DLC) and drug loading efficiency (DLE) of DOX-loaded T6 aggregates were 5.64% (for DLC) and 28.2% (for DLE), which were slightly lower than those of T6-SH aggregates (DLE = 30.8%). On this basis, the thermo-triggered drug release properties of DOX-loaded aggregates with or without additives were investigated in detail (Table S4).

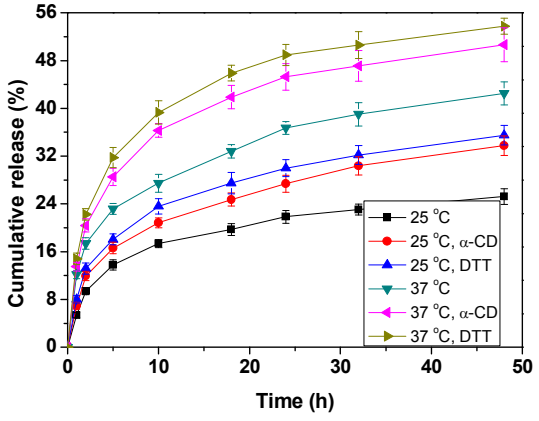

Fig. 11 In vitro drug release profiles of DOX-loaded T6 aggregates (c = 0.50 mg mL^{-1}) in PBS solution (50 mM) in the presence of 1.0 mM *α*-CD or 10 mM DTT.

To reveal the influence of temperature and additives on drug delivery properties, the in vitro drug releases from T6 aggregates were performed in PBS solution (pH 7.4, 50 mM) with or without additives at 25 or 37 °C for 48 h. The maximum release rate at a fixed temperature was liable to decrease in the order DTT > *α*-CD > lack of additives, and the apparent release rate (K) derived from the release profiles was in the range of 0.0536-0.0806 h^{-1} at 25 °C and 0.121-0.145 h^{-1} at 37 °C (Fig. 11). The cumulative release amount (CR) at 48 h was 25.2% (25 °C), 33.8% (25 °C + *α*-CD), 35.5% (25 °C + DTT), 42.5% (37 °C), 50.6% (37 °C + *α*-CD), and 53.8% (37 °C + DTT), and the increment of cumulative release (ICR, defined as the enhanced percent as compared with the lowest cumulative release amount) was in the range of 34.1-113% under different conditions. These results indicated that the release kinetics of DOX-loaded T6 aggregates could be notably adjusted in a wide range by choosing different temperatures and additives. The release rate of DOX from T6 aggregates at 37 °C was much faster than that at 25 °C, and the release kinetics could be further accelerated as additives (10 mM DTT or 1.0 mM *α*-CD) were applied, revealing the critical roles of thermo-stimulus and additives during release process. As evidenced by DLS analysis, the addition of DTT or *α*-CD could efficiently induce the copolymer aggregates to perform reaggregation or coassembly, and thus the encapsulated drug was rapidly released from the aggregates during dynamic aggregation among additives and polymer segments. Besides enhanced solubility of DOX in water at higher temperature, the destabilization and reaggregation of aggregates induced by increased hydrophobicity of PNIPAM segments and accelerated molecular mobility could account for the faster release kinetics at 37 °C.

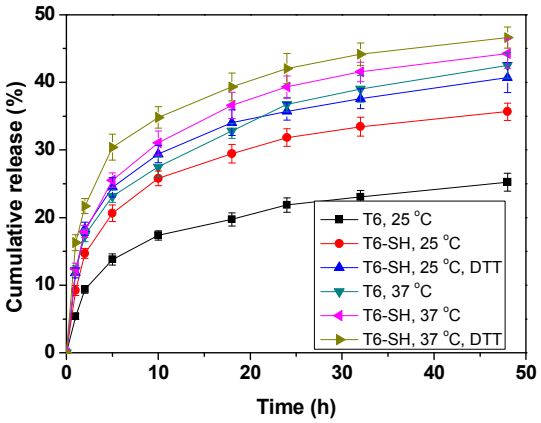

Fig. 12 In vitro drug release profiles of DOX-loaded T6 and T6-SH aggregates (c = 0.50 mg mL^{-1}) in PBS solution (50 mM) with or without addition of 10 mM DTT.

To further reveal the influence of end group, the in vitro drug releases from T6-SH aggregates were also conducted (Fig. 12). The K (h^{-1}) values were liable to decrease in the order 0.151 (T6-SH, 37 °C + DTT) ≈ 0.145 (T6, 37 °C + DTT) > 0.122 (T6-SH,

37 °C) ≈ 0.121 (T6, 37 °C) ≈ 0.118 (T6-SH, 25 °C + DTT) > 0.0910 (T6-SH, 25 °C) > 0.0806 (T6, 25 °C + DTT) > 0.0536 (T6, 25 °C), revealing T6-SH aggregates were of faster release kinetics than T6 aggregates at 25 °C although the *K* values using same conditions at 37 °C were roughly comparable. The order in cumulative release amounts at 48 h was roughly similar to that of apparent release rates except the aggregates with DTT at 37 °C. Careful inspection of release profiles in Fig. 11 and Fig. 12 revealed that CR values of aggregates using DTT at 48 h were 53.8% (for T6) and 46.6% (for T6-SH), and T6-SH aggregates were of higher cumulative release than T6 aggregates at 37 °C with time period beyond 2 h although their CR values were close within the initial 2 h. These results indicated the DOX release kinetics was significantly affected by the introduction of DTT and terminal thiol functionality, in which the continuous rearrangement and reaggregation of copolymer aggregates induced by the variable interactions among end group, additive and polymer segments could lead to faster release of the encapsulated drug.

The above-mentioned results confirmed the drug release kinetics of PNIPAM-based toothbrushlike copolymer aggregates could be tuned in a wide range by applying thermo-stimulus, variable additives and different end groups. Consequently, these copolymer aggregates had great potential as versatile nanocarriers for biomedical application. Our study further extended the application of tunable supramolecular interactions in smart drug delivery systems.

Conclusions

Novel (A-*g*-D)(B-*alt*-C)$_m$D-type toothbrushlike copolymers with three kinds of grafts and different grafting densities were efficiently synthesized by four step reactions involving quaternization and RAFT processes. The synthesized polymers possessed some topological features such as tunable grafting density and length/width ratio in terminal comblike block, densely grafted alternating grafts in middle comblike block, and multiple compositions. The physicochemical properties such as chain relaxation, melting, crystallization, and self-assembly behaviors of toothbrushlike copolymers were strongly dependnent on some factors such as macromolecular architecture, chemical composition and grafting density. Besides PNIPAM segments, the introduction of non-responsive chains into copolymers could also lead to thermo-dependent wettability of copolymer films, and this phenomenon become more pronounced as polymer segments were poorly compatible. The drug release properties of PNIPAM-based aggregates were significantly dependent on temperature, additives and end group. Our preliminary results revealed that the synthesized sequence-regulated toothbrushlike copolymers had a great potential in stimuli-sensitive surface and biomedical materials.

Acknowledgements

This work was financially supported by the National Natural Science Foundation of China (Grants 21074081 and 21274096), and the Project Funded by the Priority Academic Program Development of Jiangsu Higher Education Institutions. The authors are grateful for valuable helps from Prof. Gaojian Chen at Soochow University during DLS measurement.

Notes and references

Jiangsu Key Laboratory of Advanced Functional Polymer Design and Application, Department of Polymer Science and Engineering, College of Chemistry, Chemical Engineering and Materials Science, Soochow University, Suzhou 215123, China. Tel: +86-512-65882045; Fax: +86-512-65882045; E-mail: ylzhao@suda.edu.cn

† Electronic Supplementary Information (ESI) available: [^{1}H NMR and IR spectra, GPC traces, water contact angle photographs, DLS plots, and TEM images of copolymer aggregates]. See DOI: 10.1039/ b000000x/

1 N. Hadjichristidis, M. Pitsikalis, S. Pispas and H. Iatrou, *Chem. Rev.*, 2001, **35**, 3747−3792.
2 T. Higashihara, M. Hayashi and A. Hirao, *Prog. Polym. Sci.*, 2011, **36**, 323−375.
3 C. J. Hawker, A. W. Bosman and E. Harth, *Chem. Rev.*, 2001, **101**, 3661−3688.
4 K. Matyjaszewski and J. Xia, *Chem. Rev.*, 2001, **101**, 2921−2990.
5 M. Ouchi, T. Terashima and M. Sawamoto, *Chem. Rev.*, 2009, **109**, 4963−5050.
6 B. V. K. J. Schmidt, M. Hetzer, H. Ritter and C. Barner-Kowollik, *Prog. Polym. Sci.*, 2014, **39**, 235−249.
7 S. S. Sheiko and M. Möller, *Chem. Rev.*, 2001, **101**, 4099−4123.
8 S. S. Sheiko, B. S. Sumerlin and K. Matyjaszewski, *Prog. Polym. Sci.*, 2008, **33**, 759−785.
9 H.-i. Lee, J. Pietrasik, S. S. Sheiko and K. Matyjaszewski, *Prog. Polym. Sci.*, 2010, **35**, 24−44.
10 C. Feng, Y. J. Li, D. Yang, J. H. Hu, X. H. Zhang and X. Y. Huang, *Chem. Soc. Rev.*, 2011, **40**, 1282−1295.
11 Y. M. Chen, *Macromolecules*, 2012, **45**, 2619−2631.
12 H. F. Shi, Y. Zhao, X. Dong, Y. Zhou and D. J. Wang, *Chem. Soc. Rev.*, 2013, **42**, 2075−2099.
13 K. Huang and J. Rzayev, *J. Am. Chem. Soc.*, 2009, **131**, 6880–6885.
14 M. Müllner, T. Lunkenbein, M. Schieder, A. H. Gröschel, N. Miyajima, M. Förtsch, J. Breu, F. Caruso and A. H. E. Müller, *Macromolecules*, 2012, **45**, 6981−6988.
15 Z. C. Zheng, A. Daniel, W. Yu, B. Weber, J. Ling and A. H. E. Müller, *Chem. Mater.*, 2013, **25**, 4585−4594.
16 I. Park, S. S. Sheiko, A. Nese and K. Matyjaszewski, *Macromolecules*, 2009, **42**, 1805–1807.
17 Y. C. Li, A. Nese, N. V. Lebedeva, T. Davis, K. Matyjaszewski and S. S. Sheiko, *J. Am. Chem. Soc.*, 2011, **133**, 17479–17484.
18 Y. C. Li, A. Nese, K. Matyjaszewski and S. S. Sheiko, *Macromolecules*, 2013, **46**, 7196−7201.
19 M. Wintermantel, M. Gerle, K. Fischer, M. Schmidt, I. Wataoka, H. Urakawa, K. Kajiwara and Y.Tsukahara, *Macromolecules*, 1996, **29**, 978−983.
20 M. Gerle, K. Fischer, S. Roos, A. H. E. Müller, M. Schmidt, S. S. Sheiko, S. Prokhorova and M. Moller, *Macromolecules*, 1999, **32**, 2629−2637.
21 B. Zhang, F. Grohn, J. S. Pedersen, K. Fischer and M. Schmidt, *Macromolecules*, 2006, **39**, 8440−8450.
22 S. S. Sheiko, F. C. Sun, A. Randall, D. Shirvanyants, M. Rubinstein, H. Lee and K. Matyjaszewski, *Nature*, 2006, **440**, 191−194.
23 T. Stephan, S. Muth and M. Schmidt, *Macromolecules*, 2002, **35**, 9857−9860.
24 J. G. Kim and G. W. Coates, *Macromolecules*, 2012, **45**, 7878–7883.
25 Y. Xia, B. D. Olsen, J. A. Kornfield and R. H. Grubbs, *J. Am. Chem. Soc.*, 2009, **131**, 18525−18532.
26 G. M. Miyake, R. A. Weitekamp, V. A. Piunova and R. H. Grubbs, *J. Am. Chem. Soc.*, 2012, **134**, 14249–14254.
27 N. Cakir, M. Yavuzarslan, H. Durmaz, G. Hizal and U. Tunca, *J. Polym. Sci, Part A: Polym. Chem.*, 2013, **51**, 899−907.
28 J. A. Johnson, Y. Y. Lu, A. O. Burts, Y.-H. Lim, M. G. Finn, J. T. Koberstein, N. J. Turro, D. A. Tirrell and R. H. Grubbs, *J. Am. Chem. Soc.*, 2011, **133**, 559–566.
29 I. Gadwal, J. Y. Rao, J. Baettig and A. Khan, *Macromolecules*, 2014, **47**, 35−40.
30 M. M. Caruso, D. A. Davis, Q. Shen, S. A. Odom, N. R. Sottos, S. R. White and J. S. Moore, *Chem. Rev.*, 2009, **109**, 5755–5798.

31 D. Roy, J. N. Cambre and B. S. Sumerlin, *Prog. Polym. Sci.*, 2010, **35**, 278–301.
32 N. Badi and J.-F. Lutz, *Chem. Soc. Rev*., 2009, **38**, 3383−3390.
33 J.-F. Lutz, M. Ouchi, D. R. Liu and M. Sawamoto, *Science*, 2013, **341**, 1238149.
34 Y. Hibi, M. Ouchi and M. Sawamoto, *Angew. Chem., Int. Ed*., 2011, **50**, 7434−7437.
35 K. Nakatani, Y. Ogura, Y. Koda, T. Terashima and M. Sawamoto, *J. Am. Chem. Soc*., 2012, **134**, 4373−4383.
36 J. Zhang, M. E. Matta and M. A. Hillmyer, *ACS Macro Lett.*, 2012, **1**, 1383−1387.
37 G. Gody, T. Maschmeyer, P. B. Zetterlund and S. Perrier, *Nature Commun.*, 2013, **4**, 2505.
38 K. Satoh, M. Matsuda, K. Nagai and M. Kamigaito, *J. Am. Chem. Soc*., 2010, **132**, 10003−10005.
39 M. Matsuda, K. Satoh and M. Kamigaito, *Macromolecules*, 2013, **46**, 5473−5482.
40 Z.-L. Li, L. Li,F.-S. Du and Z.-C. Li, *Chinese J. Polym. Sci*., 2013, **31**, 355−362.
41 C.-H. Wang, Z.-Y. Song, X.-X. Deng, L.-J. Zhang, F.-S. Du and Z.-C. Li, *Macromol. Rapid Commun.*, 2014, **35**, 474−478.
42 J. J. Yan, D. Wang, D. C. Wu and Y. Z. You, *Chem. Commun.*, 2013, **49**, 6057−6059.
43 G. H. Deng and Y. M. Chen, *J. Polym. Sci., Part A: Polym. Chem.*, 2009, **47**, 5527−5533.
44 Y. H. Zhang, J. Huang and Y. M. Chen, *Macromolecules*, 2005, **38**, 5069−5077.
45 Y. H. Zhang, Z. Z. Xu, X. K. Li and Y. M. Chen, *J. Polym. Sci., Part A: Polym. Chem*., 2007, **45**, 3994−4001.
46 H. Zhu, G. H. Deng and Y. M. Chen, *Polymer*, 2008, **49**, 405−411.
47 A. O. Moughton, T. Sagawa, W. M. Gramlich, M. Seo, T. P. Lodge and M. A. Hillmyer, *Polym. Chem.*, 2013, **4**, 166–173.
48 S. X. Li, C. N. Ye, G. D. Zhao, M. J. Zhang and Y. L. Zhao, *J. Polym. Sci., Part A: Polym. Chem.*, 2012, **50**, 3135−3148.
49 X. Jiang, W. Shao, K. Jiang. M. J. Zhang, H. H. Liu, C. N. Ye and Y. L. Zhao, *Polym. Chem.*, 2013, **4**, 3272−3281.
50 X. Jiang, M. J. Zhang, S. X. Li, W. Shao and Y. L. Zhao, *Chem. Commun.*, 2012, **48**, 9906−9908**.**
51 M. J. Zhang, H. H. Liu, W. Shao, K. Miao and Y. L. Zhao, *Macromolecules*, 2013, **46**, 1325−1336.
52 Y. Y. Mai and A. Eisenberg, *Chem. Soc. Rev.*, 2012, 41, 5969−5985.
53 Z. B. Li, E. Kesselman, Y. Talmon, M. A. Hillmyer and T. P. Lodge, *Science*, 2004, **306**, 98−101.
54 T. P. Lodge, A. Rasdal, Z. B. Li and M. A. Hillmyer, *J. Am. Chem. Soc*., 2005, **127**, 17608−17609.
55 A. O. Moughton, M. A. Hillmyer and T. P. Lodge, *Macromolecules*, 2012, **45**, 2−19.
56 A. H. Gröschel, F. H. Schacher, H. Schmalz, O. V. Borisov, E. B. Zhulina, A. Walther and A. H. E. Müller, *Nature Commun*., 2012, **3**, 710.
57 G. Sun, H. Cui, L. Y. Lin, N. S. Lee, C. Yang, W. L. Neumann, J. N. Freskos, J. J. Shieh, R. B. Dorshow and K. L. Wooley, *J. Am. Chem. Soc*., 2011, **133**, 8534−8543.
58 C. Weber, M. Wagner, D. Baykal, S. Hoeppener, R. M. Paulus, G. Festag, E. Altuntas, F. H. Schacher and U. S. Schubert, *Macromolecules*, 2013, **46**, 5107−5116.
59 P. E. Theodorakis, W. Paul and K. Binder, *Macromolecules*, 2010, **43**, 5137−5148.
60 J. Chiefari, Y. K. Chong, F. Ercole, J. Krstina, J. Jeffery, T. P. T. Le, R. T. A. Mayadunne, G. F. Meijs, C. L. Moad, G. Moad, E. Rizzardo and S. H. Thang, *Macromolecules*, 1998, **31**, 5559−5562.
61 M. J. Zhang, H. H. Liu, W. Shao, C. N. Ye and Y. L. Zhao, *Macromolecules*, 2012, **45**, 9312−9325.
62 Y. Mitsukami, M. S. Donovan, A. B. Lowe and C. L. McCormick, *Macromolecules*, 2001, **34**, 2248−2256.
63 G. Mantovani, F. Lecolley, L. Tao, D. M. Haddleton, J. Clerx, J. J. L. M. Cornelissen and K. Velonia, *J. Am. Chem. Soc*., 2005, **127**, 2966−2973.
64 K. Miao, W. Shao, H. H. Liu and Y. L. Zhao, *Polym. Chem*., 2014, **5**, 1191–1201.
65 G. A. Ilevbare, H. Y. Liu, J. Pereira, K. J. Edgar and L. S. Taylor, *Mol. Pharm.*, 2013, **10**, 3392–3403.
66 A. Srinatha and J. K. Pandit, *Drug Delivery*, 2008, **15**, 471–476.
67 M.-S. Kim, J.-S. Kim, S.-H. Kang, Y.-H. Yoo, S. Lee, J.-S. Park, J.-S. Woo and S.-J. Hwang, *Arch. Pharm. Res.*, 2007, **30**, 1008–1013.
68 J. Li and X. J. Loh, *Adv. Drug Del. Rev*., 2008, **60**, 1000–1017.
69 A. L. Laza-Knoerr, R. Gref and P. Couvreur, *J. Drug Targ*., 2010, **18**, 645–656.
70 G. S. Chen and M. Jiang, *Chem. Soc. Rev*., 2011, **40**, 2254–2266.
71 J. X. Zhang and P. X. Ma, *Adv. Drug Del. Rev*., 2013, **65**, 1215–1233.
72 J. Z. Du, H. Willcock, J. P. Patterson, I. Portman and R. K. O'Reilly, *Small*, 2011, **7**, 2070–2080.
73 S. Chhabra, V. Sachdeva and S. Singh, *Int. J. Pharm*., 2007, **342**, 72–77.
74 S. Meng, Z. Guo, Q. Wang, Z. J. Liu, Q. H. Wang, W. Zhong and Q. G. Du, *J. Biomater. Sci. Polym. Ed.*, 2011, **22**, 651–664.
75 J. Z. Du and R. K. O'Reilly, *Chem. Soc. Rev*., 2011, **40**, 2402–2416.
76 H. Liu and S. S. Venkatraman, *J. Biomater. Sci. Polym. Ed*., 2012, **23**, 251–266.
77 B. Chen, K. Jerger, J. M. J. Fréchet and F. C. Sazka Jr, *J. Control. Release*, 2009, **140**, 203–209.
78 M. Parent, C. Nouvel, M. Koerber, A. Sapin, P. Maincent and A. Boudier, *J. Control. Release*, 2013, **172**, 292–304.
79 S. Venkataraman, J. L. Hedrick, Z. Y. Ong, C. Yang, P. L. R. Ee, P. T. Hammond and Y. Y. Yang, *Adv. Drug Del. Rev.*, 2011, **63**, 1228–1246.
80 W. Shao, K. Miao, H. H. Liu, C. N. Ye, J. Z. Du and Y. L. Zhao, *Polym. Chem*., 2013, **4**, 3398–3410.

Graphical Abstract:

Synthesis and properties of heterografted toothbrushlike copolymers with alternating PEG and PCL grafts and tunable RAFT-generated segments

Dandan Tang, Xiao Jiang, Huanhuan Liu, Cangxia Li and Youliang Zhao

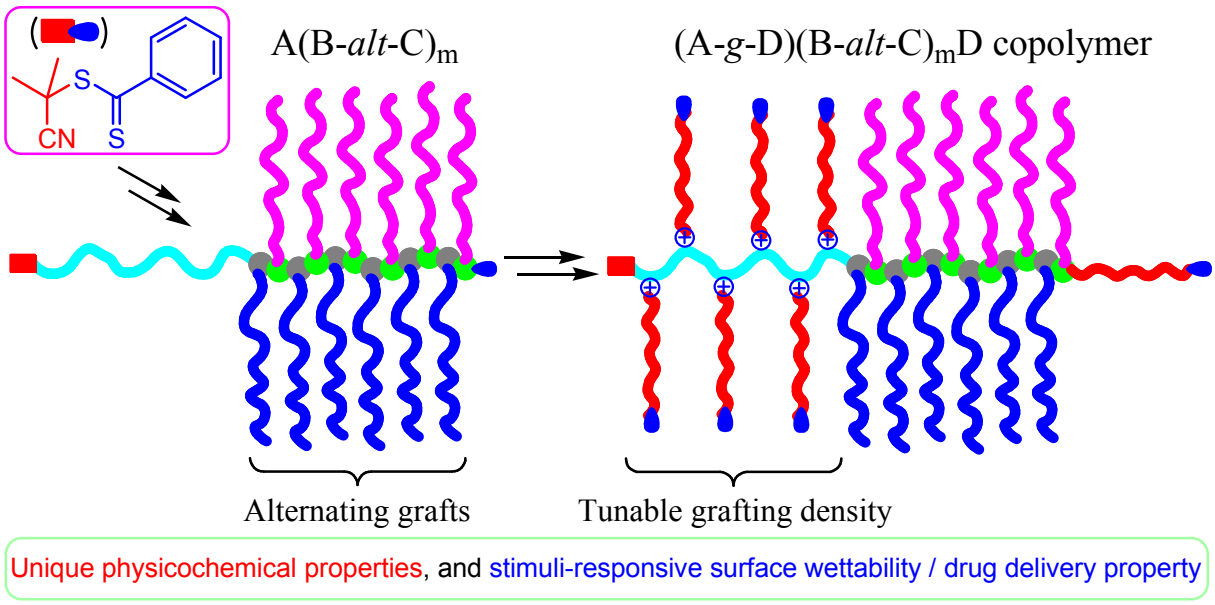

Novel (A-*g*-D)(B-*alt*-C)$_m$D-type heterografted toothbrushlike copolymers with great potential in smart drug delivery systems and thermo-responsive surface materials were investigated.